

Dependence of the solar cell performance on nanocarbon/Si heterojunctions

Shiqi Xiao(肖仕奇), Qingxia Fan(范庆霞), Xiaogang Xia(夏晓刚), Zhuojian Xiao(肖卓建), Huiliang Chen(陈辉亮), Wei Xi(席薇), Penghui Chen(陈鹏辉), Junjie Li(李俊杰), Yanchun Wang(王艳春), Huaping Liu(刘华平), Weiya Zhou(周维亚)

Citation: Chin. Phys. B . 2018, 27(7): 078801. **doi:** 10.1088/1674-1056/27/7/078801

Journal homepage: http://cpb.iphy.ac.cn; http://iopscience.iop.org/cpb

What follows is a list of articles you may be interested in

Detection of invisible phonon modes in individual defect-free carbon nanotubes by gradient-field Raman scattering

Feng Yang(杨丰), Yinglu Ji(纪英露), Xiao Zhang(张霄), Qingxia Fan(范庆霞), Nan Zhang(张楠), Xiaogang Gu(谷孝刚), Zhuojian Xiao(肖卓建), Qiang Zhang(张强), Yanchun Wang(王艳春), Xiaochun Wu(吴晓春), Junjie Li(李俊杰), Weiya Zhou(周维亚)

Chin. Phys. B . 2017, 26(7): 078801. **doi:** 10.1088/1674-1056/26/7/078801

Design and optimization of carbon nanotube/polymer actuator by using finite element analysis

Wei Zhang(张薇), Luzhuo Chen(陈鲁倬), Jianmin Zhang(张健敏), Zhigao Huang(黄志高)

Chin. Phys. B . 2017, 26(4): 048801. **doi:** 10.1088/1674-1056/26/4/048801

Performance improvement of continuous carbon nanotube fibers by acid treatment

Qiang Zhang(张强), Kewei Li(李克伟), Qingxia Fan(范庆霞), Xiaogang Xia(夏晓刚), Nan Zhang(张楠), Zhuojian Xiao(肖卓建), Wenbin Zhou(周文斌), Feng Yang(杨丰), Yanchun Wang(王艳春), Huaping Liu(刘华平), Weiya Zhou(周维亚)

Chin. Phys. B . 2017, 26(2): 028802. **doi:** 10.1088/1674-1056/26/2/028802

Flexible impedance and capacitive tensile load Sensor based on CNT composite

Zubair Ahmad, Kh S Karimov, Farid Touati

Chin. Phys. B . 2016, 25(2): 028801. **doi:** 10.1088/1674-1056/25/2/028801

Novel pressure and displacement sensors based on carbon nanotubes

Kh. S. Karimov, Khaulah Sulaiman, Zubair Ahmad, Khakim M. Akhmedov, A. Mateen

Chin. Phys. B . 2015, 24(1): 018801. **doi:** 10.1088/1674-1056/24/1/018801

Dependence of the solar cell performance on nanocarbon/Si heterojunctions*

Shiqi Xiao(肖仕奇)[1,3], Qingxia Fan(范庆霞)[1,3], Xiaogang Xia(夏晓刚)[1,3], Zhuojian Xiao(肖卓建)[1,3], Huiliang Chen(陈辉亮)[1,3], Wei Xi(席薇)[1,3], Penghui Chen(陈鹏辉)[1,3], Junjie Li(李俊杰)[1,3], Yanchun Wang(王艳春)[1,2,3], Huaping Liu(刘华平)[1,2,3], and Weiya Zhou(周维亚)[1,2,3,†]

[1] *Beijing National Laboratory for Condensed Matter Physics, Institute of Physics, Chinese Academy of Sciences, Beijing* 100190, *China*
[2] *Beijing Key Laboratory for Advanced Functional Materials and Structure Research, Beijing* 100190, *China*
[3] *University of Chinese Academy of Sciences, Beijing* 100049, *China*

(Received 17 April 2018; published online 25 June 2018)

Solar cells that combine single-crystalline silicon (Si) with graphene (G) have been widely researched in order to develop next-generation photovoltaic devices. However, the power conversion efficiency (PCE) of G/Si solar cell without chemical doping is commonly low due to the relatively high resistance of graphene. In this work, through combining graphene with carbon nanotube (CNT) networks, we fabricated three kinds of hybrid nanocarbon film/Si heterojunction solar cells in order to increase the PCE of the graphene based Si solar cell. We investigated the characteristics of different nanocarbon film/Si solar cells and found that their performance depends on the heterojunctions. Specifically, a doping-free G-CNT/Si solar cell demonstrated a high PCE of 7.9%, which is nearly equal to the combined value of two individuals (G/Si and CNT/Si). This high efficiency is attributed to the synergistic effect of graphene and CNTs, and can be further increased to 9.1% after applying a PMMA antireflection coating. This study provides a potential way to further improve the Si based heterojunction solar cells.

Keywords: carbon nanotube, graphene, heterojunction, silicon solar cell

PACS: 88.30.rh, 81.05.ue, 73.40.Lq, 88.40.jj **DOI:** 10.1088/1674-1056/27/7/078801

1. Introduction

Graphene (G), an atomically thick two-dimensional nanocarbon material, has attracted increasing attention in the development of next-generation photovoltaic devices due to its excellent electrical, optical, and chemical stable properties.[1–6] In particular, solar cells that combine crystalline silicon (Si) with graphene synthesized by the chemical vapor deposition (CVD) method have shown promising potential because of the simple and low-cost fabrication process.[7–9] In a typical G/Si heterojunction solar cell, the graphene film not only participates in the formation of the heterojunction, but also serves as the window electrode and hole collector.[9–11] When the device is illuminated, the incident light passes through the graphene and creates electron–hole pairs in the Si substrate.[12] The generated electron–hole pairs are then separated by the built-in electric field. Afterwards, the separated holes diffuse across the graphene film in the lateral direction to be collected. Hence, good transparency and conductivity of the graphene film are of high importance to obtain the expected solar cell with high power conversion efficiency (PCE).

However, due to the polycrystalline feature of CVD-graphene and cracks or residues formed in the polymer-assisted transfer processes, the obtained graphene films commonly show relatively high sheet resistance in the range of several hundreds to thousands of Ω/sq.[13–18] When applied in the Si solar cells, the high sheet resistance of graphene not only causes severely charged carrier recombination, but also brings about serious power loss. For instance, Ho *et al.*[15] reported that the relatively low conductivity of graphene (990 Ω/sq) leads to a low fill factor (FF) of the G/Si solar cell, which results in a low PCE of 3.3%. Similarly, a G/Si solar cell with a PCE of 3.47% was also reported based on graphene with sheet resistance of 1500 Ω/sq.[16] Chemical doping of graphene can yield enhanced FF and open circuit voltage of the G/Si solar cells.[11,14,19] However, the doped solar cells face the problem of fast degradation,[9] which greatly influences their developments.

Recently, many studies have focused on the assembly of graphene with carbon nanotube (CNT), which yields new types of nanocarbon materials with diverse structure characteristics and different properties.[20–24] On the one hand, high strength one-dimensional CNTs can reinforce the atomically thin graphene film, which is conductive to the polymer-free transfer process.[21] On the other hand, the hybrid films of graphene and CNTs have shown better conductiv-

*Project supported by the National Key R&D Program of China (Grant No. 2018YFA0208402), the National Basic Research Program of China (Grant No. 2012CB932302), the National Natural Science Foundation of China (Grant Nos. 11634014, 51172271, and 51372269), the Strategic Priority Research Program of the Chinese Academy of Sciences (Grant No. XDA09040202).

†Corresponding author. E-mail: wyzhou@iphy.ac.cn

© 2018 Chinese Physical Society and IOP Publishing Ltd

ity compared to an individual graphene or CNT film, making them more adoptable for flexible transparent conductive electrodes.[18,22,23] Apart from the hybrid films, the native oxides on Si have also been proved to greatly affect the characteristics of as fabricated heterojunction solar cells by controlling the magnitude of the thermionic emission dark current.[14,25] However, the optimal oxides for different heterojunctions require different thicknesses.[26–28] Our previous report has also shown that, in a PEDOT:PSS-CNT/Si solar cell, the optimal oxide thickness between PEDOT:PSS/Si heterojunction is thinner compared to that of CNTs/Si, which brings about the difficulty in the design of an oxide layer to fulfill the needs for both PEDOT:PSS and CNT based Si solar cells.[29] Considering the similar sp^2 hybridization structure and properties of graphene and CNTs, their optimal oxide thicknesses are almost the same. These features provide a lot of convenience for us to construct the high efficiency Si solar cells based on graphene and CNTs.

In this work, we improved the G/Si solar cell efficiency through hybridizing graphene with CNTs and investigated the performance of the hybrid films with diverse assembly configurations in Si solar cells. Specifically, three types of hybrid films based on graphene and CNT network were assembled, including G/CNT and CNT/G hybrid films, which were fabricated by simple stacking CNT network on graphene, as well as a coplanar nanostructure (G-CNT film) synthesized by a chemical vapor deposition (CVD) method. We found that the solar cell performance depends on the nanocarbon/Si heterojunction. The G-CNT/Si solar cell, in which there are both G/Si and CNT/Si contact heterojunctions, exhibits better *J*–*V* characteristics than the ones with a single type of contact. Its high efficiency (PCE = 7.9%) is attributed to the synergistic effect of graphene and CNTs. After applying a PMMA antireflection coating, the PCE of the as-fabricated PMMA/G-CNT/Si solar cell can be further improved to 9.1%. These findings illustrate the dependence of the Si solar cell performance on different nanocarbon materials and provide a potential way to further enhance the efficiency of this type of solar cells.

2. Experimental details

2.1. Preparation of different nanocarbon materials

Graphene film was grown by Cu-catalyzed low-pressure chemical vapor deposition (LPCVD) method using H_2 and CH_4.[30] The Cu foil (46365, from Alfa Aesar) was first treated with ammonium persulfate to remove the native oxides, then cleaned with acetone, ethanol, and deionized water successively. The cleaned Cu foil was then loaded into a quartz tube and the system was pumped to vacuum. Then the tube was put inside a furnace and heated to 1020 °C in the atmosphere of H_2 (15 sccm). Next, 1 sccm CH_4 was introduced with the H_2 gas flow rate unchanged. After 10 min growth, the furnace was turned off and the quartz tube was cooled down to ambient temperature.

To assemble the CNT/G hybrid film, a transparent and conductive freestanding CNT network film, in which the CNT bundles are interconnected well with each other by Y-type junctions, was transferred onto the graphene/Cu substrate.[31] Then a drop of ethanol was used to enhance the contact of CNTs and graphene. After drying, the Cu substrate was dissolved in the ammonium persulfate solution, leaving a free standing CNT-G hybrid film. To obtain the G/CNT hybrid film, the CNT/G hybrid film was carefully flipped over to the other side.

The preparation process of the coplanar G-CNT hybrid film is similar to that employed in an earlier report.[32] A piece of continuous CNT network was first transferred onto a pretreated Cu foil (46365, from Alfa Aesar), then placed in the quartz tube and the quartz tube was evacuated. The following procedures are the same as the growth procedures of graphene described above. The sample was then taken out from the quartz tube and floated on the ammonium persulfate solution to dissolve Cu. Finally, a G-CNT hybrid film floated on the solution was obtained.

2.2. Fabrication of solar cells

N-type silicon wafer (100) with resistivity of 1–3 Ω·cm and 300 nm SiO_2 were used to fabricate solar cells. The wafer was first patterned to square windows by ultraviolet photolithography and the exposed SiO_2 was etched in BOE solution, leaving a bare fresh Si surface (3 mm×3 mm). After that, the Si substrate was washed with acetone and ethanol for several times. To obtain an optimal oxide layer, the Si substrate was immersed in dilute nitric acid (0.5 M) for 40 s. Different nanocarbon materials were then transferred onto the substrates to form different junctions. Afterwards, silver paste was painted around the active window while eutectic gallium-indium (EGaIn, from Alfa Aesar) was applied to the back side of Si to form the cathode.

2.3. Characterization

Raman spectra were recorded using LabRAM HR 800 (HORIBA Jobin Yvon Inc.) with a 514 nm laser. An atomic force microscope (AFM, Bruker MultiMode-8 ScanAsyst) was used to characterize the surface morphology of different nanocarbon materials. The optical transmission was measured with a Shimadzu UV-3600 UV–Vis–NIR spectrophotometer. A handheld four-probe meter (Tonghui, TH2661) was used to measure the sheet resistance of different nanocarbon materials. The performance of a solar cell was measured using a solar simulator (Perfectlight CHF-XM 500) under AM 1.5 G

with a calibrated irradiation intensity of 100 mW/cm^2. The J–V data were recorded with a Keithley 4200-SCS.

3. Results and discussion

Figure 1 shows the schematic fabrication processes of the three different kinds of hybrid films based on graphene and CNTs. The different fabrication methods determined the resulting configurations of the hybrid films. For the G/CNT or CNT/G hybrid films, the high-strength CNT network synthesized via a developed CVD method was coated on the graphene (grown on Cu foil) directly. Owing to the freestanding feature of the CNT network and the strong Van der Waals force between graphene and CNTs, a freestanding hybrid film could be formed after the Cu foil was dissolved.[20] For the fabrication of the G-CNT hybrid film, the CNT network was first coated on bare Cu foil, followed by growth of graphene. After the Cu foil was removed, a freestanding coplanar G-CNT hybrid film could be obtained, as shown in Fig. 1(b).

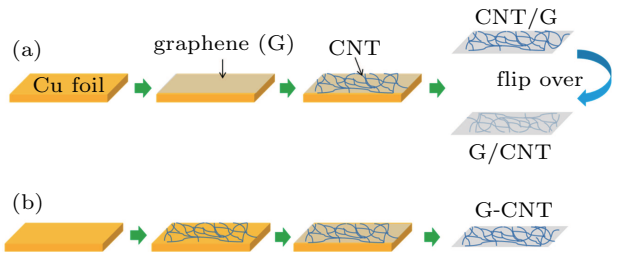


Fig. 1. (color online) Schematic fabrication processes of graphene and CNT based hybrid films with different configurations: (a) CNT/G and G/CNT hybrid films, (b) coplanar G-CNT hybrid film.

In the Raman spectra of different nanocarbon materials, as shown in Fig. 2(a), a high quality CNT network exhibits typical radial breathing mode (RBM), D band, G band, and 2D band, with the intensity ratio of D to G bands smaller than 0.05. For the as-grown graphene, no D band or RBM band, a G band ($\sim$ 1590 cm^{-1}) with a single Lorentzian feature, and a strong 2D band ($\sim$ 2690 cm^{-1}) are observed, which indicates the single-layer feature of graphene.[33] On the other hand, the Raman spectra of different hybrid films are almost the same. The existence of RBM and the overview Raman spectra illustrate the coexistence of CNTs and graphene. Moreover, very weak D bands, in both the CNT/G (G/CNT) and G-CNT hybrid films, indicate that the fabrication processes did not bring obvious defects.

Figure 2(b) shows the optical transmittances of the as-grown CVD graphene film, CNT network, G/CNT (CNT/G), and G-CNT hybrid films with the corresponding sheet resistances. The transmittance at 550 nm of the as-grown single-layer graphene and the CNT network is 99.6% (780 Ω/sq) and 89.2% (270 Ω/sq), respectively. The assembled hybrid films, however, show a slight decrease in transmittance compared to the CNT network due to overlaying of graphene. Typically, the G/CNT or CNT/G hybrid film exhibits a transmittance of 87.1%, which is almost the same as that of the G-CNT hybrid film (85.8%). The hybrid films have lower sheet resistance than an individual graphene film and CNT network. The sheet resistance of the obtained G/CNT (CNT/G) and G-CNT hybrid films is 210 Ω/sq and 190 Ω/sq, respectively. This decrease is mainly attributed to the additional charge transport channel in the graphene and CNT network assemblies.[23]

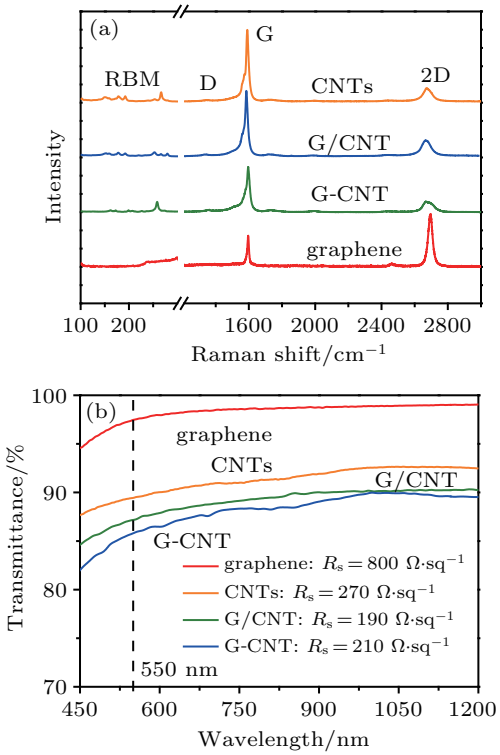


Fig. 2. (color online) (a) Raman spectra of graphene, CNT network, G/CNT, and G-CNT films. (b) Optical transmittance and sheet resistance of typical graphene, CNT network, G/CNT, and G-CNT films on glass substrates. Due to the same nanostructures of the G/CNT and CNT/G hybrid films, their Raman spectra, optical transmittances, and sheet resistances are nearly the same.

From the surface morphology of each hybrid film on a SiO_2 (300 nm)/Si substrate characterized by AFM (Fig. 3), it is evident that all three free-standing hybrid films have complete structures after the transfer processes, which proves their high mechanical strength. At the same time, obvious difference can also be observed between the G/CNT hybrid film and the other two hybrid films. For a G/CNT hybrid film (Fig. 3(b)), the upper graphene film acts as a soft and smooth "blanket" which covers the CNT network, hence giving rise to no noticeable CNTs' morphology. For the CNT/G and G-CNT hybrid films (Figs. 3(a) and 3(c)), the sharp and clear height variations of the CNT network are very obvious, which are distinct compared to the G/CNT hybrid film. Moreover, owing to the strengthened effect of a continuous CNT network, the graphene counterparts in the hybrid films are almost integral.

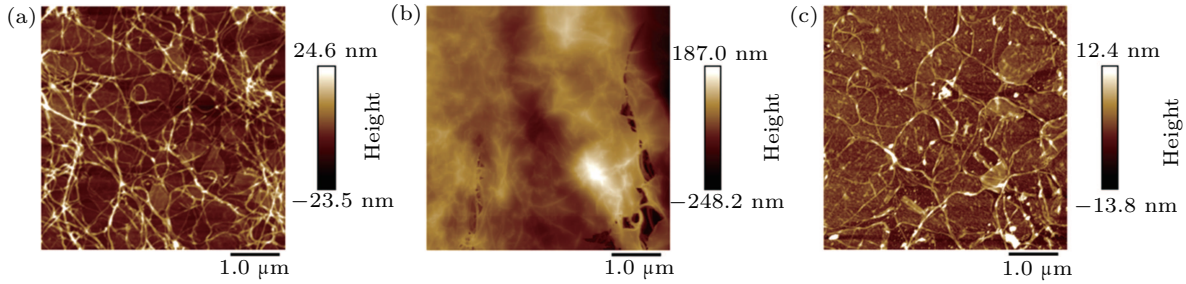


Fig. 3. (color online) AFM images of (a) CNT/G, (b) G/CNT, and (c) G-CNT films on Si substrates.

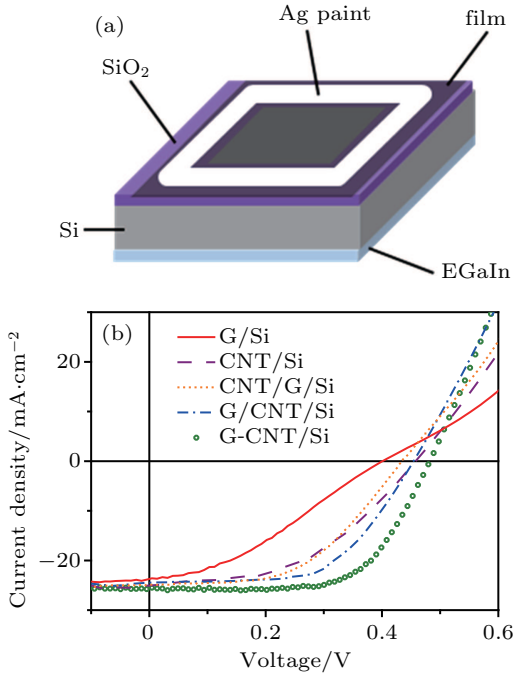


Fig. 4. (color online) (a) Structure diagram of a nanocarbon film/Si solar cell. (b) Representative *J*–*V* characteristics of different solar cells based on graphene, CNT network, G/CNT hybrid, CNT/G hybrid, and G-CNT hybrid films.

In order to investigate the performance of different nanocarbon films applied in Si based solar cells, the films were transferred onto n-type single crystalline Si substrates to form heterojunctions (junction area is 9 mm^2 for all devices). The structure of the as-designed nanocarbon film/Si heterojunction solar cell is depicted in Fig. 4(a). The nanocarbon films served as the anode electrode and were surrounded by silver paint, whereas the cathode was constructed with EGaIn. Depending on the heterojunctions formed with Si, the resulted devices are denoted as G/Si, CNT/Si, G/CNT/Si, CNT/G/Si, and G-CNT/Si solar cells. The *J*–*V* curves of different types of solar cells tested under 1 sun condition ($P_{input} = 100\ mW{\cdot}cm^{-2}$, AM 1.5 illumination) are shown in Fig. 4(b). Briefly, the solar cells with hybrid film window electrodes perform better than the G/Si and CNT/Si solar cells. Specifically, the G/Si solar cell exhibits a short circuit current density (J_{sc}) of 23.6 $mA{\cdot}cm^{-2}$, an open circuit voltage (V_{oc}) of 400 mV, and a fill factor (FF) of 34.9%, which results in a PCE of 3.3% (Table 1). This result is consistent with the results in the earlier reports.[15,16] Besides, the CNT/G/Si solar cell shows an enhanced J_{sc} of 24.9 $mA{\cdot}cm^{-2}$, V_{oc} of 427 mV, FF of 52.7%, and PCE of 5.6%. A similar result is obtained in the CNT/Si (PCE = 5.4%) and G/CNT/Si (6.5%) solar cells. Among all these devices, the G-CNT/Si solar cell possesses the highest PCE (7.9%), which shows a J_{sc} of 25.5 $mA{\cdot}cm^{-2}$, V_{oc} of 480 mV, and FF of 64.5%.

Furthermore, the series resistance (R_s) and ideality factor (n) are calculated under the dark measurements with the following equation:[14]

$$\frac{dV}{d\ln I} = R_s I + \frac{nkT}{q}, \tag{1}$$

where q is the elementary electric charge, and k is the Boltzmann constant. The calculated R_s and n are listed in Table 1. Also noteworthy is that the G/Si solar cell has the highest R_s (47 Ω) and n (2.5) while the G-CNT/Si solar cell shows the smallest R_s (21 Ω) and n (1.8).

Table 1. Comparison of device parameters of different Si based heterojunction solar cells with graphene, CNT network, G/CNT, CNT/G, and G-CNT hybrid films as the top electrodes.

Device	J_{sc}/mA·cm^{-2}	V_{oc}/mV	FF/%	PCE/%	R_s/Ω	n
G/Si	23.6	400	34.9	3.3	47	2.5
CNT/Si	24.9	458	47.4	5.4	29	2.1
G/CNT/Si	24.4	452	58.9	6.5	25	2.0
CNT/G/Si	24.9	427	52.7	5.6	31	2.2
G-CNT/Si	25.5	480	64.5	7.9	21	1.8

In fact, the majority of reported graphene grown by the CVD method shows a sheet resistance of about 1000 Ω/sq, which is much larger than its theoretical value (30 Ω/sq).[34] Unlike the freestanding CNT network, the graphene grown on copper catalyst substrate needs to be protected in the course of transfer. The commonly used method is spin coating a thin PMMA layer on the graphene to serve as a protective sacrifice layer.[30] However, cracks and polymer residues are often formed in this process (Fig. 5(a)), which severely degrade the original properties of the graphene film.[17] Moreover, the grain boundaries in polycrystalline graphene also reduce the conductivity of the graphene film.[18] In the presence of defects and residues (Fig. 5(b)), the photon-generated charge carriers will be scattered and recombined, resulting in a poor performance of the G/Si solar cell. This is consistent with its high

R_s and n calculated above (Table 1). When the CNT network is hybridized with graphene, the CNT network can provide more pathways for the charge carriers, which leads to the improved conductivity. The enhanced conductivity of the hybrid film results in less power loss of the solar cell, which brings about higher FF and V_{oc} compared to those of the G/Si solar cells. This improvement is reflected in the reduced R_s and n of the hybrid nanocarbon film/Si solar cells.

Interestingly, the PCE of the G-CNT/Si solar cell is higher than that of the G/CNT/Si and CNT/G/Si solar cells. As the sheet resistance and optical transmittance of these hybrid films are almost the same, the only difference is the heterojunction formed with Si. For the G/CNT or CNT/G hybrid films, there only exists one type of heterojunction (G/Si heterojunction or CNT/Si heterojunction). However, because of the hybridization method employed for the hybrid films, the graphene and CNTs contact the Si together in the G-CNT/Si solar cell, jointly forming two types of heterojunctions, as shown in Fig. 5(c). In particular, the G/Si heterojunction is established to be a Schottky junction, as many works reported.[11,14] But there still exist some divergences on the heterojunction type of CNT/Si due to a mixture of semiconducting and metallic CNTs in a typical CVD synthesized CNT film. For instance, Jia *et al.*[35] reported that the CNT/Si contact is a Schottky heterojunction. Jung *et al.*[26] studied the temperature dependence of a CNT/Si solar cell and suggested that the CNT/Si contact is a p–n heterojunction. As reported earlier,[29] our CNT/Si solar cell is similar to the latter as a whole. Accordingly, the measured PCE of the G-CNT/Si solar cell (7.9%) is almost equal to the sum of those of a CNT/Si (5.4%) and a G/Si solar cell (3.3%), and nearly twice that of the solar cell with a similar structure reported earlier.[36] By analyzing the dependence of the solar cell performance on three kinds of nanocarbon film/Si heterojunctions, it is evident that the coexistence of G/Si and CNT/Si heterojunctions in the G-CNT/Si solar cell gives rise to a larger contact area compared to the CNT/Si or G/CNT/Si solar cells, resulting in the enhanced collecting ability of holes. Besides, once the photo-generated holes are extracted to the G-CNT hybrid film, the charge carriers can be transported more efficiently by a continuous high conductive CNT network with Y-type CNT interconnection.[29] Therefore, the G-CNT hybrid architecture finally results in much less scattering events from the defects and impurities in the graphene film. These features can be concluded as the synergistic effect of graphene and CNT network in the as-designed G-CNT/Si solar cell.

The stability of the G-CNT/Si solar cell is further studied (Fig. 6(a)). Over 15-day storage at room temperature and ambient atmosphere, the solar cell retained 94% PCE of the original value, which shows very stable performance. To further enhance its efficiency, a thin PMMA layer, which served as the antireflection coating, was spin coated on its surface. As shown in Fig. 6(b), the resulted solar cell demonstrated an enhanced PCE of 9.1%. This improvement is mainly attributed to the increased short circuit current (30 mA·cm^{-2}), almost 16% higher than the pristine value.

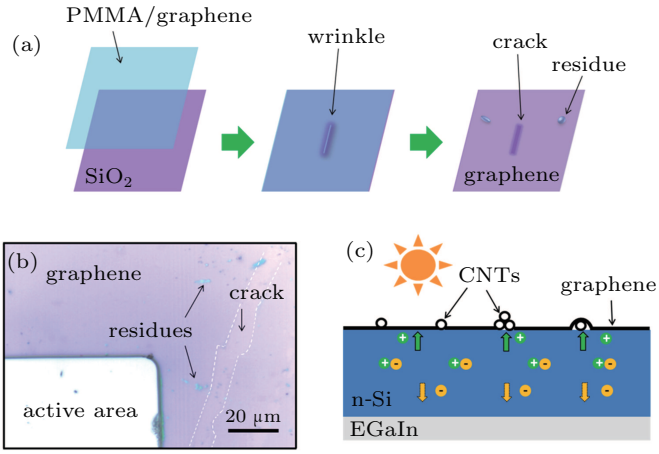


Fig. 5. (color online) (a) Schematic diagram of the formation of cracks and residues in the transfer process. (b) Optical microscope image of as-fabricated G/Si solar cell. A dash-line crack of graphene can be observed by the different contrast of graphene and SiO_2. (c) Mechanism graph of the photovoltaic process. The separated holes are collected by both CNTs and graphene individuals.

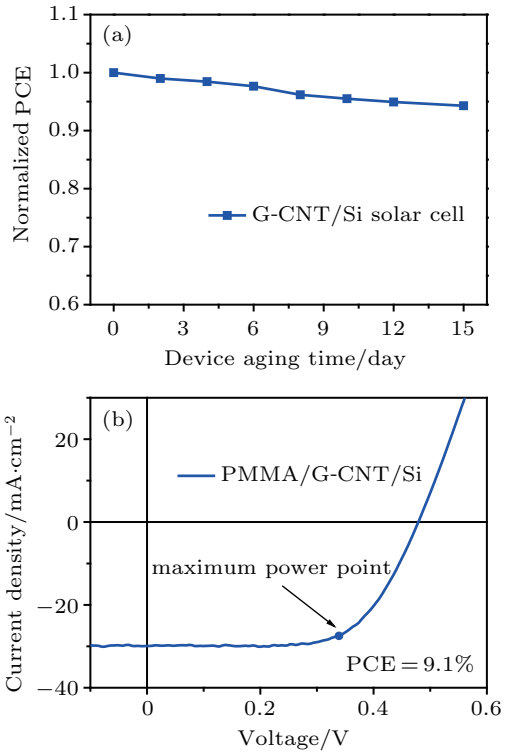


Fig. 6. (color online) (a) Time dependence of PCE of a G-CNT/Si solar cell. (b) *J*–*V* characteristics of G-CNT/Si solar cell coated with a moderate layer of PMMA (PMMA/G-CNT/Si for short).

4. Conclusions

We have analyzed the characteristics of doping-free G/Si solar cells and found that the relatively poor performance re-

sults from the high resistance of the CVD-derived graphene film. Through the introduction of a continuous and conductive CNT network, we designed three types of hybrids with different configurations, which all showed much better conductivity than graphene. As a result, a Si solar cell with a high and stable PCE of 7.9% without chemical doping was fabricated based on a coplanar G-CNT hybrid film. The PCE was improved by about 46% and 139% compared to those of the individual CNT/Si (5.4%) and G/Si (3.3%) solar cells fabricated at the same condition. By investigating the characteristics of different nanocarbon film/Si solar cells, we revealed the dependence of their performance on the heterojunctions formed in the devices. On the one hand, the efficiency improvement of the G-CNT/Si solar cell is attributed to the same optimal interfacial oxide thickness of G/Si heterojunction and CNT/Si heterojunction, which makes it feasible to obtain optimal heterojunction quality simultaneously. On the other hand, the coexistence of G/Si and CNT/Si heterojunctions in the G-CNT/Si photovoltaic device exhibits a synergistic effect, resulting in more carrier transport paths and more efficient carrier collection. Finally, the device efficiency was further enhanced to 9.1% after applying a PMMA antireflection coating. Our work also reveals new aspects of the device architecture and the potential for Si based heterojunction photovoltaic devices.

Acknowledgment

The author H. P. L. thanks support by the Recruitment Program of Global Youth Experts and the “100 talents project” of CAS.

References

[1] Bae S, Kim H, Lee Y, Xu X, Park J S, Zheng Y, Balakrishnan J, Lei T, Kim H R, Song Y I, Kim Y J, Kim K S, Ozyilmaz B, Ahn J H, Hong B H and Iijima S 2010 *Nat. Nanotech.* **5** 574
[2] Wang Y, Tong S W, Xu X F, Ozyilmaz B and Loh K P 2011 *Adv. Mater.* **23** 1514
[3] Park H, Brown P R, Bulovic V and Kong J 2012 *Nano Lett.* **12** 133
[4] Weiss N O, Zhou H, Liao L, Liu Y, Jiang S, Huang Y and Duan X 2012 *Adv. Mater.* **24** 5782
[5] Jang H, Park Y J, Chen X, Das T, Kim M S and Ahn J H 2016 *Adv. Mater.* **28** 4184
[6] Sun D M, Liu C, Ren W C and Cheng H M 2016 *Adv. Electron. Mater.* **2** 1600229
[7] Li X, Zhu H, Wang K, Cao A, Wei J, Li C, Jia Y, Li Z, Li X and Wu D 2010 *Adv. Mater.* **22** 2743
[8] Shi E, Li H, Yang L, Zhang L, Li Z, Li P, Shang Y, Wu S, Li X, Wei J, Wang K, Zhu H, Wu D, Fang Y and Cao A 2013 *Nano Lett.* **13** 1776
[9] Li X, Lv Z and Zhu H 2015 *Adv. Mater.* **27** 6549
[10] Li X, Xie D, Park H, Zeng T H, Wang K, Wei J, Zhong M, Wu D, Kong J and Zhu H 2013 *Adv. Energy Mater.* **3** 1029
[11] Miao X, Tongay S, Petterson M K, Berke K, Rinzler A G, Appleton B R and Hebard A F 2012 *Nano Lett.* **12** 2745
[12] Kozawa D, Hiraoka K, Miyauchi Y, Mouri S and Matsuda K 2012 *Appl. Phys. Express* **5** 042304
[13] Kang J, Shin D, Bae S and Hong B H 2012 *Nanoscale* **4** 5527
[14] Song Y, Li X, Mackin C, Zhang X, Fang W, Palacios T, Zhu H and Kong J 2015 *Nano Lett.* **15** 2104
[15] Ho P H, Liou Y T, Chuang C H, Lin S W, Tseng C Y, Wang D Y, Chen C C, Hung W Y, Wen C Y and Chen C W 2015 *Adv. Mater.* **27** 1724
[16] Xu W, Deng B, Shi E, Wu S, Zou M, Yang L, Wei J, Peng H and Cao A 2015 *ACS Appl. Mater. Inter* **7** 17088
[17] Lin Y C, Lu C C, Yeh C H, Jin C, Suenaga K and Chiu P W 2012 *Nano Lett.* **12** 414
[18] Cummings A W, Duong D L, Nguyen V L, Van Tuan D, Kotakoski J, Barrios Vargas J E, Lee Y H and Roche S 2014 *Adv. Mater.* **26** 5079
[19] Li X, Xie D, Park H, Zhu M, Zeng T H, Wang K, Wei J, Wu D, Kong J and Zhu H 2013 *Nanoscale* **5** 1945
[20] Lin X, Liu P, Wei Y, Li Q, Wang J, Wu Y, Feng C, Zhang L, Fan S and Jiang K 2013 *Nat. Commun.* **4** 2920
[21] Yan Z, Peng Z, Casillas G, Lin J, Xiang C, Zhou H, Yang Y, Ruan G, Raji A R O, Samuel E L G, Hauge R H, Yacaman M J and Tour J M 2014 *ACS Nano* **8** 5061
[22] Kim S H, Song W, Jung M W, Kang M A, Kim K, Chang S J, Lee S S, Lim J, Hwang J, Myung S and An K S 2014 *Adv. Mater.* **26** 4247
[23] Kholmanov I N, Magnuson C W, Piner R, Kim J Y, Aliev A E, Tan C, Kim T Y, Zakhidov A A, Sberveglieri G, Baughman R H and Ruoff R S 2015 *Adv. Mater.* **27** 3053
[24] Wang R, Hong T and Xu Y Q 2015 *ACS Appl. Mater. Inter* **7** 5233
[25] Pulfrey D L 1978 *IEEE Trans. Electron. Devices* **25** 1308
[26] Jung Y, Li X, Rajan N K, Taylor A D and Reed M A 2013 *Nano Lett.* **13** 95
[27] Cui K, Anisimov A S, Chiba T, Fujii S, Kataura H, Nasibulin A G, Chiashi S, Kauppinen E I and Maruyama S 2014 *J. Mater. Chem. A* **2** 11311
[28] He J, Gao P, Yang Z, Yu J, Yu W, Zhang Y, Sheng J, Ye J, Amine J C and Cui Y 2017 *Adv. Mater.* **29**
[29] Fan Q, Zhang Q, Zhou W, Xia X, Yang F, Zhang N, Xiao S, Li K, Gu X, Xiao Z, Chen H, Wang Y, Liu H, Zhou W and Xie S 2017 *Nano Energy* **33** 436
[30] Li X, Cai W, An J, Kim S, Nah J, Yang D, Piner R, Velamakanni A, Jung I, Tutuc E, Banerjee S K, Colombo L and Ruoff R S 2009 *Science* **324** 1312
[31] Fan Q, Zhang Q, Zhou W, Yang F, Zhang N, Xiao S, Gu X, Xiao Z, Chen H, Wang Y, Liu H and Zhou W 2017 *Chin. Phys. B* **26** 028801
[32] Shi E, Li H, Yang L, Hou J, Li Y, Li L, Cao A and Fang Y 2015 *Adv. Mater.* **27** 682
[33] Ferrari A C and Basko D M 2013 *Nat. Nanotech.* **8** 235
[34] Griep M H, Sandoz-Rosado E, Tumlin T M and Wetzel E 2016 *Nano Lett.* **16** 1657
[35] Jia Y, Li P, Gui X, Wei J, Wang K, Zhu H, Wu D, Zhang L, Cao A and Xu Y 2011 *Appl. Phys. Lett.* **98** 133115
[36] Shi E, Li H, Xu W, Wu S, Wei J, Fang Y and Cao A 2015 *Nano Energy* **17** 216